Model Independent Determination of HWW coupling and Higgs total width at ILC

Claude Dürig[a], Keisuke Fujii[b], Jenny List[a], Junping Tian[b]

[a] *Deutsches Elektronen-Synchrotron (DESY), Hamburg, Germany*
[b] *High Energy Accelerator Research Organization (KEK), Tsukuba, Japan*

This article is based on the talk presented at the International Workshop on Future Linear Colliders (LCWS13) which held during November 11-15, 2013 at Tokyo, Japan. We present several analyses related to the Higgs total width study at ILC based on the full detector simulation of ILD, which are $e^+e^- \to \nu\bar{\nu}H$ followed by $H \to b\bar{b}$ and $H \to WW^*$. The studies show that at 250 GeV we can determine the Higgs total width with a relative precision of 11% and the HWW coupling with 4.8%, whereas at 500 GeV the expected precision can be significantly improved to 5% and 1.2% respectively, assuming the baseline integrated luminosities of ILC, which are 250 fb^{-1} @ 250 GeV, 500 fb^{-1} @ 500 GeV, and a beam polarization of $P(e^-, e^+) = (-80\%, +30\%)$. A new approach of removing pile-up particles based on multivariate method developed during those analyses is also presented.

arXiv:1403.7734v1 [hep-ex] 30 Mar 2014

Contents

I. Introduction 1

II. Simulation Framework 3

III. Analysis of $\sigma_{\nu\bar{\nu}H} \times \mathrm{Br}(H \to b\bar{b})$ @ 250 GeV 3

IV. Analysis of $\sigma_{\nu\bar{\nu}H} \times \mathrm{Br}(H \to b\bar{b})$ @ 500 GeV 5

A. Removal of Overlay 6

B. Event selection and reduction table 8

V. Analysis of $\sigma_{\nu\bar{\nu}H} \times \mathrm{Br}(H \to WW^*)$ @ 500 GeV 8

A. $WW^* \to$ 4-jets 9

B. $WW^* \to l\nu +$ 2-jets 9

C. Combined of $H \to WW^*$ with full hadronic and semi-leptonic modes 11

VI. Summary 11

Acknowledgments 12

References 12

I. INTRODUCTION

Following the discovery of a Standard Model (SM) like Higgs boson with a mass around 125 GeV, the determination of its total decay width is one of the fundamental physical tasks of investigating its profile. For an SM Higgs of this mass, the expected total width is around 4 MeV, which is far beyond the detector resolution at both LHC and ILC and therefore it cannot be measured directly by reconstructing its line shape. So some indirect approaches are proposed in the references [1–4]. Consequently, at LHC, due to the fact that it's impossible to measure the Higgs decay inclusively, the Higgs total width cannot be determined model independently. At ILC, the advantage of recoil mass techniques make the inclusive measurement possible. It measures the absolute cross section of $e^+e^- \to ZH$, which is proportional

to the square of the HZZ coupling (g_Z^2). With g_Z^2 known, the partial width of $H \to ZZ^*$ (Γ_Z) can be given explicitly. Combined with another measurement of the branching ratio of $H \to ZZ^*$ (BR_Z), the Higgs total width (Γ_H) can be determined by

$$\Gamma_H = \frac{\Gamma_Z}{\mathrm{BR}_Z}.$$

In this approach Γ_Z can be measured accurately, however for the SM Higgs the precision of BR_Z is statistically limited by its small branching ratio BR_Z∼2.7%. Another approach by utilizing the $H \to WW^*$ mode, which has a much larger branching ratio BR_W∼ 22%, gives

$$\Gamma_H = \frac{\Gamma_W}{\mathrm{BR}_W}.$$

The determination of Γ_W or g_W^2 is not as trivial as in the case of Γ_Z. To explain the method, let's look at the following five independent observables:

$$\begin{aligned}
Y_1 &= \sigma_{ZH} = F_1 \cdot g_Z^2 \\
Y_2 &= \sigma_{ZH} \times \mathrm{Br}(H \to b\bar{b}) = F_2 \cdot \frac{g_Z^2 g_b^2}{\Gamma_H} \\
Y_3 &= \sigma_{\nu\bar{\nu}H} \times \mathrm{Br}(H \to b\bar{b}) = F_3 \cdot \frac{g_W^2 g_b^2}{\Gamma_H} \\
Y_4 &= \sigma_{\nu\bar{\nu}H} \times \mathrm{Br}(H \to WW^*) = F_4 \cdot \frac{g_W^4}{\Gamma_H} \\
Y_5 &= \sigma_{ZH} \times \mathrm{Br}(H \to WW^*) = F_5 \cdot \frac{g_Z^2 g_W^2}{\Gamma_H},
\end{aligned}$$

where g_Z, g_W and g_b are the couplings of Higgs to ZZ, WW and $b\bar{b}$ respectively; F_1, F_2, F_3, F_4 and F_5 are factors which we can calculate unambiguously [5–7] (though there are some theory errors either from higher order corrections or from errors of parameters such as m_H or m_b, those errors are believed to be well controlled below the sub-percent level). With these five observables the couplings and the total width can be obtained as following:

i.) from the measurement Y_1 we can get the coupling $g_Z = \sqrt{\frac{Y_1}{F_1}}$.

ii.) from the ratio Y_2/Y_3 we can get the coupling ratio $g_Z/g_W = \sqrt{\frac{Y_2}{Y_3}\frac{F_3}{F_2}}$.

iii.) with g_Z and g_Z/g_W, we can get $g_W = \sqrt{\frac{Y_1 Y_3}{Y_2}\frac{F_2}{F_1 F_3}}$.

iv.) **option A**: once we know g_W, from the measurement Y_4 we can get the Higgs total width $\Gamma_H = \frac{Y_1^2 Y_3^2}{Y_2^2 Y_4}\frac{F_2^2 F_4}{F_1^2 F_3^2}$;
option B: once we know g_Z and g_W, from the measurement Y_5 we can get the Higgs total width $\Gamma_H = \frac{Y_1^2 Y_3}{Y_2 Y_5}\frac{F_2 F_5}{F_1^2 F_3}$.

These two options are constrained by both the Higgs-strahlung $e^+e^- \to ZH$ and the WW-fusion $e^+e^- \to \nu\bar{\nu}H$ production processes. At 250 GeV, the former one reaches its maximum cross section, but latter has a small cross section, thus making option B the more suitable method. The main limiting factor arises from the precision of the measurement Y_3. Going up to 500 GeV, the WW-fusion production cross section is around one order larger compared to 250 GeV, which makes option A the better option. It is worth emphasizing that eventually the precisions of $2\frac{\Delta Y_1}{Y_1}$ and $\frac{\Delta Y_4}{Y_4}$ limit the precision of the total width, since Y_2 usually is far better measured than Y_1, and Y_3 twice better than Y_4.

In this article, we focus on the analyses of measuring the observables Y_3 and Y_4 through the WW-fusion channel. The analyses for Y_1, Y_2 and Y_3 through the Higgs-strahlung channel have been investigated in [8–10]. At both 250 GeV and 500 GeV, $Y_3 = \sigma_{\nu\bar{\nu}H} \times \mathrm{Br}(H \to b\bar{b})$ is studied since it is mandatory in option A and option B; $Y_4 = \sigma_{\nu\bar{\nu}H} \times \mathrm{Br}(H \to WW^*)$ is studied only at 500 GeV since it is useless at 250 GeV, and both the hadronic and semi-leptonic decay of WW^* are investigated.

Nevertheless, the determination of deviation of HWW coupling to its SM value itself has important impact on the existence of additional Higgs boson [11, 12]. In the $W_L W_L \to W_L W_L$ scattering process, the unitarity is insured

by the HWW coupling which is constrained to be $2m_W^2/v$ in SM. If deviation smaller to its SM value is found, it strongly indicates that there exists another neutral heavier Higgs boson which also contributes to the scattering process. Depending on the size of deviation, if it's around 1%, it suggests the new heavier Higgs mass would be lighter than 10 TeV, and if it's around 10%, the new heavier Higgs mass would be lighter than 2 TeV. However, if it turns out that deviation larger than SM value is found, interesting enough is the indication that there exists double charged new Higgs boson with similar scale constraints as the formal deviation case. So the precision measurement of HWW coupling would provide strong indication of next energy scale we need explore.

II. SIMULATION FRAMEWORK

All the signal and background samples for 500 GeV analyses are generated using the common DBD softwares [13], and LoI softwares [14] for 250 GeV analysis, based on the full detector simulation of ILD by GEANT4. WHIZARD [15] is used as event generator, detector simulation is done by Mokka [16], and reconstruction is done by Marlin [17]. Particle flow is carried out by PandoraPFA [18], package LCFIPlus [19] and LCFIVertex[20] are used to provide flavor tagging information.

III. ANALYSIS OF $\sigma_{\nu\bar{\nu}H} \times \mathrm{Br}(H \to b\bar{b})$ @ 250 GEV

The feasibility of the measurement of the Higgs production cross section through WW-fusion is investigated for $\sqrt{s} = 250$ GeV and a beam polarization of $P(e^+e^-) = (0.3, -0.8)$, assuming $250\,\mathrm{fb}^{-1}$ of data. We can extract information on the coupling g_W of the Higgs boson to W-bosons which then provides us the possibility to determine the total decay width of the Higgs boson. The SM Higgs boson with a mass below 140 GeV is expected to decay predominantly into two b-quarks

$$e^+e^- \longrightarrow \nu_e\bar{\nu}_e H \longrightarrow \nu_e\bar{\nu}_e b\bar{b}\,.$$

In the $H\nu_e\bar{\nu}_e$ final state, Higgs-strahlung and WW-fusion cannot be taken separately as non-interfering. The WW-fusion cross-section increases logarithmically to large $\sqrt{s}$, whereas Higgs-strahlung scales as s^{-1}. Hence and due to the enhanced cross section at the threshold $\sqrt{s} = m_\mathrm{H} + m_\mathrm{Z}$ Higgs-strahlung diagrams give the dominant contribution to the combined process at low energies and thus representing one of the most challenging backgrounds in the analysis. Next to Higgs-strahlung, backgrounds considered in this search mode are two-fermion events, having a production cross-section which is more than 1000 times larger than the signal cross-section, semi-leptonically and hadronically decaying Z/W-pairs, and single Z/W-boson production processes. Background events from two-photon processes are found to be negligible. The cross-section of the two-photon interaction is very large, but their particular features allow to suppress them at an early stage of the analysis. The backgrounds are divided into the following types: $b\bar{b}\nu_l\bar{\nu}_l$, $q\bar{q}\nu_l\bar{\nu}_l$ ($q \neq b$), $q\bar{q}\nu_l l$, $q\bar{q}l^-l^+$, $q\bar{q}q\bar{q}$ and $q\bar{q}$. The large background contribution around $\sqrt{s} = 250$ GeV make the analysis very challenging. The signal search mode consists of missing four-momentum and two energetic, very forward b-jets. In the beginning of the analysis all reconstructed particles are clustered into two jets representing the Higgs decay products. The event selection is performed in three stages. The first step involves pre-cuts, using the number of charged tracks N_ctrk and the removal of isolated leptons in the events. Since the neutrino mode is selected, there are no signal events containing isolated leptons. In the signal leptons appear in the jets at most. Removing events with isolated leptons leads to a reduction of semi-leptonic backgrounds $q\bar{q}l^+l^-$ and $q\bar{q}l\nu_l$. Background events originating from hadronic decays of W- and Z-pairs, as well as $q\bar{q}$-pairs, can contain more particles compared to the WW-fusion signal. The introduced limits on the number of charged tracks in an event $10 \leq N_\mathrm{ctrk} \leq 40$ help to reduce $q\bar{q}l^+l^-$, $q\bar{q}q\bar{q}$ and $q\bar{q}$ background and exclude fully leptonic events for sure. The second stage of the event selection contains cuts on kinematic variables and in the third stage more event specific cuts are performed, mainly using jet characteristics and variables resulting from jet clustering and flavor tagging. In the following, the selection cuts are discussed briefly:

- Cut1: visible mass has to be consistent with $m_\mathrm{H} - 20\ \mathrm{GeV} \leq m_\mathrm{vis} \leq m_\mathrm{H} + 10\ \mathrm{GeV}$. It has a great effect on the $q\bar{q}$-background since ISR photons, which are preferably emitted in beam-pipe direction and might escape detection faking missing energy, can bring the invariant visible mass of the two-fermion system back to $m_\mathrm{vis} \approx m_\mathrm{Z}$. Even though the invariant mass of the $q\bar{q}$-background peaks at m_Z, the tail of the visible mass distribution is still large, leaving this the dominant background. Additionally, W- or Z-pair background get rejected well.

- Cut2: visible energy is required to be 105 GeV $\leq E_{\text{vis}} \leq$ 160 GeV. This selection cut is not very effective, mainly reducing $q\bar{q}$-background.
- Cut3: absolute value of visible and invisible transverse momentum p_{T} are equal due to momentum conservation. In backgrounds without neutrinos ($q\bar{q}l^+l^-$, $q\bar{q}q\bar{q}$, $q\bar{q}$) missing p_{T} can be caused by particles that stay undetected. Hence, those backgrounds mainly consist of events with low p_{T}. A requirement on the total transverse momentum 20 GeV $\leq \sum p_{\text{T}} \leq$ 80 GeV reduces backgrounds without neutrinos in the final state.
- Cut4 & Cut5: the Durham jet clustering algorithm offers two variables Y_{23} and Y_{12}. These parameters are useful to discriminate between events with different numbers of jets. Events have to satisfy $Y_{23} \leq 0.02$, which is the threshold value to reconstruct two jets as three jets. To further discriminate between signal and background, a cut on the second parameter is applied $0.2 \leq Y_{12} \leq 0.8$, which corresponds to the minimum Y-parameter at which the number of jets changes from two to one for the two-jet hypothesis.
- Cut6: flavor tagging is performed by using the LCFIVertex flavor tagging package. It is based on a neutral net approach to distinguish b-, c- and light jets. The b-jet likelihood should fulfill btag ≥ 0.85. Due to the near absence of b-quarks in backgrounds originating from W- and Z-bosons, these processes can be reduced.
- Cut7: total jets momentum in beam direction should satisfy $|\sum p_{\text{z}}| \leq 60$ GeV. Since the W- and Z-boson in the corresponding backgrounds are relatively boosted, p_{z} is larger as compared to WW-fusion and Higgs-strahlung events. The cut is very helpful to reduce a large part of the two-fermion background contribution.
- Cut8: Z- and W-bosons are produced at small angles from the e^+e^--beams and therefore the angular distribution of these processes have peaks in the forward and backward regions. A cut on $|\cos(\theta_{\text{jet}})| \leq 0.95$ is applied.

During the event selection, more cuts have been tested to further reduce background, without the desired effect. The Higgs-strahlung and WW-fusion distribution of the different cut parameters are most of the time of similar shape thus making the choice of cuts less effective for Higgs-strahlung events. The effect of each cut on signal and background events are listed in table I.

TABLE I: The reduction table for the signal and backgrounds in the analysis of $\nu\bar{\nu}H \to \nu\bar{\nu}b\bar{b}$ at 250 GeV. The cut names are explained in the text. $\nu\bar{\nu}H$ is divided into WW-fusion and Higgs-strahlung.

Process	expected	pre-selection	Cut1	Cut2	Cut3	Cut4	Cut5	Cut6	Cut7	Cut8
$\nu\bar{\nu}H$(fusion)	3426	2663	2070	2023	1577	1053	965	547	519	507
$\nu\bar{\nu}H(ZH)$	1.4×10^4	10918	8356	8356	7448	4860	4594	2574	2546	2546
$\nu_l\bar{\nu}_l b\bar{b}$	3.05×10^4	23012	1040	1040	878	421	390	224	193	187
$\nu_l\bar{\nu}_l q\bar{q}$	1.19×10^5	88998	5548	5545	4714	2408	2271	15	9	9
$q\bar{q}l^+l^-$	2.99×10^5	153540	6196	5922	1760	588	508	65	38	36
$q\bar{q}l\nu$	1.73×10^6	1.15×10^6	181973	177193	134047	22654	20533	111	73	65
$q\bar{q}q\bar{q}$	3.91×10^6	1.15×10^6	782	728	3	1	0	0	0	0
$q\bar{q}$	26.02×10^6	17.27×10^6	852321	794892	1507	1199	683	289	152	152
BG	32.104×10^6	19.846×10^6	1.047×10^6	985320	142909	27271	24385	1404	465	449

After the selection, the dominant background to WW-fusion is represented by Higgs-strahlung. The remaining background contribution is in the same order as the signal. In order to determine the WW-fusion cross section, we modify the relation $\sigma_{\nu\bar{\nu}H}(H \to b\bar{b}) = \sigma_{\nu\bar{\nu}H} \times BR(H \to b\bar{b})$ to

$$\sigma_{\nu\bar{\nu}H} \times BR(H \to b\bar{b}) = \frac{N'_{\text{WW}}}{\epsilon \cdot \mathcal{L}}\,, \tag{1}$$

where ϵ is the selection efficiency and $\mathcal{L}$ the integrated luminosity. It follows, that by extracting the number of WW-fusion events N'_{WW} which have passed the event selection, $\sigma_{\nu\bar{\nu}H} \times BR(H \to b\bar{b})$ can be determined. The WW-fusion events with $\nu\bar{\nu}b\bar{b}$ final state can be separated from the corresponding one in Higgs-strahlung by exploiting their different characteristics in the $\nu\bar{\nu}$ invariant mass, which are measurable through the missing mass distribution. Therefore, a χ^2-fit is applied on the shape of the missing mass distribution consisting of the remaining WW-fusion, Higgs-strahlung and background events and by using Toy Monte Carlo data as reference. In a χ^2-fit, the function

$$\chi^2 = \sum_i^{N_{\text{bins}}} (N_i^{\text{pred}} - N_i^{\text{data}})^2 / \sigma^2(N_i^{\text{pred}}),$$

has to be minimized, where N_i^{data} and N_i^{pred} is the number of data and predicted events in bin i. In order to fit on the missing mass distribution consisting of background, Higgs-strahlung and WW-fusion, we need to set up N_i^{pred} as a function of the three distributions:

$$N_i^{\text{pred}} = f_{\text{WW}} N'_{\text{WW},i} + f_{\text{ZH}} N'_{\text{ZH},i} + f_{\text{bgrd}} N'^{\text{tot}}_{\text{bgrd},i},$$

where $N'_{\text{WW},i}$, $N'_{\text{ZH},i}$ and $N'^{\text{tot}}_{\text{bgrd},i}$ represent the number of events in bin i after the selection, respectively. The parameters $f_{\text{WW}}, f_{\text{ZH}}$ and f_{bgrd} are adjusted so as to minimize the χ^2-function.

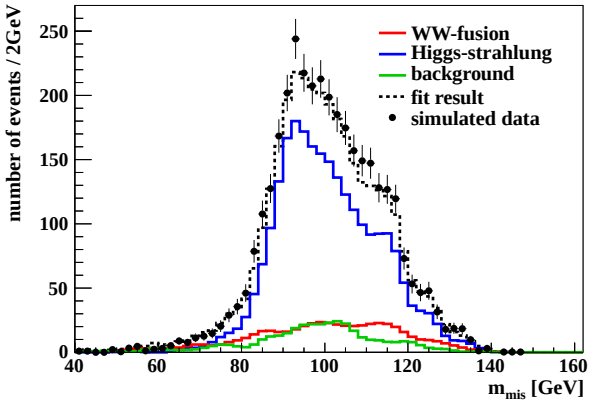

FIG. 1: Missing mass distribution of WW-fusion, Higgs-strahlung and background for $m_{\text{H}} = 125$ GeV after cuts, including the fit result. The shape of the Higgs-strahlung distribution is expected to peak at m_{Z}, whereas WW-fusion is expected to peak at slightly larger missing masses for 250 GeV. Latter is quasi-flat due to the small number of WW-fusion events.

The result of the fit yields the cross-section $\sigma_{\nu\bar{\nu}H}(H \to b\bar{b})$, since only $H \to b\bar{b}$ decays are selected. This is a simplified assumption assuming only true b-jet particles have passed the event selection. The fit result depicted in figure 1 states as results:

Process	$N'_{\text{WW}} \pm \Delta N'_{\text{WW}}$	$N'_{\text{ZH}} \pm \Delta N'_{\text{ZH}}$	$N'^{\text{tot}}_{\text{bgrd}} \pm \Delta N'^{\text{tot}}_{\text{bgrd}}$
Fit result	512 ± 54	$2\,497 \pm 85$	454 ± 46

The relative precision of $\sigma_{\nu\bar{\nu}H} \times BR(H \to b\bar{b})$ can be determined by using gaussian error propagation of Equation 1. The uncertainty in the efficiency is considered negligible. Systematic effects of the luminosity are not considered in the analysis. Taking into account the uncertainties from the fit and from the branching ratio measurement, the precision of $\sigma_{\nu\bar{\nu}H} \times BR(H \to b\bar{b})$ is expected to be 10.5 %.

IV. ANALYSIS OF $\sigma_{\nu\bar{\nu}H} \times \text{Br}(H \to b\bar{b})$ @ 500 GEV

The analysis of this mode at 500 GeV is quite similar to the one at 250 GeV, except that the cross section of $e^+e^- \to \nu\bar{\nu}H$ through WW-fusion is almost one order larger at 500 GeV, ~ 150 fb. High statistics of signal events which are due to the large cross section and the large branching ratio of $H \to b\bar{b}$, offer the opportunity of a precision measurement. The signal final state consists of two missing neutrinos and two b-jets. For the pre-selection, it is natural to reconstruct two jets from all reconstructed particles, and to reject events with isolated charged leptons. This efficiently suppresses the backgrounds such as those including leptonic decays of W or Z. Each event, either signal or background, is overlaid with beam induced $\gamma\gamma \to$ hadrons events [21]. The cross section of this overlay increases significantly as the center-of-mass energy rises. At 500 GeV, an average of 1.7 $\gamma\gamma \to$ hadrons events per bunch crossing is estimated. So before using the inclusive jet clustering algorithm, some methods are used to remove the overlaid particles from those we are interested in.

The dominant background processes considered in this analysis are 4-fermion processes from $e^+ + e^- \to \nu\bar{\nu}Z$, ZZ, $e\nu W$, W^+W^-, and 6-fermion processes mainly from $e^+ + e^- \to t\bar{t}$. For the final selection, we require large missing energies and missing Pt to significantly suppress the fully hadronic backgrounds. The reconstructed jets need to be tagged as b-jets which significantly suppresses the light-quark jet backgrounds. In order to separate

the signal contribution from $e^+e^- \to ZH$, a missing mass larger than the Z-boson mass is required. Distributions of those related variables after pre-selection for both signal and backgrounds are plotted in figure 2. After the final selection, figure 3 gives the distribution of the reconstructed Higgs invariant mass, where both the Higgs peak from the signal and the Z peak from $\nu\bar{\nu}Z$ can be seen clearly. Eventually, a cut on the Higgs invariant mass is applied to suppress the $\nu\bar{\nu}Z$ background.

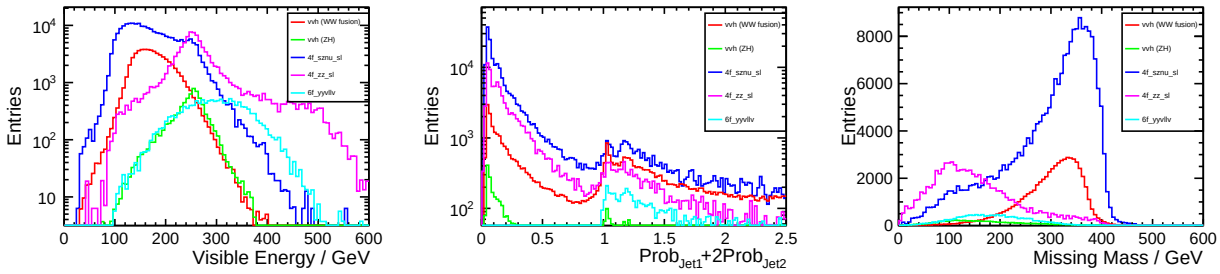

FIG. 2: Distributions of visible energy (left), b-likeness (middle) and missing mass (right) for signal $\nu\bar{\nu}H$ and backgrounds, where 4f_sznu_sl is for 4-fermions from $\nu\bar{\nu}Z \to \nu\bar{\nu}qq$, 4f_zz_sl is for 4-fermions from $ZZ \to \nu\bar{\nu}qq$ and 6f_yyvllv is mainly 6-fermions from the leptonic decay of $t\bar{t}$.

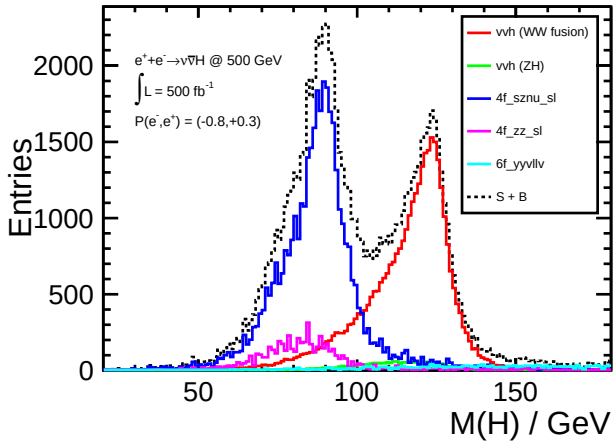

FIG. 3: Distribution of the reconstructed Higgs invariant mass using $H \to b\bar{b}$.

A. Removal of Overlay

Two methods are developed to remove particles originating from the overlaid beam background. One of them is based on the k_T or anti-k_T jet clustering algorithm. The overlaid particles usually have very low Pt and a large polar angle in the forward and backward regions which is very close to beam direction. This usually makes distances defined in the k_T or anti-k_T algorithm between overlaid particles and particles from the target process very large. Hence the beam background particles can be effectively un-selected by the jet clustering. The R value is optimized to get the best Higgs mass resolution after the overlay removal, which is shown in figure 4 (left). This method usually works well for target processes with high Pt hard jets, for instance $H \to b\bar{b}$ in this analysis where R is optimized to be 1.5.

Instead of using the method based on jet clustering, another particle based approach can be used, in which the overlaid particles are tagged one by one from the information on Pt and the polar angle. In addition, the IP information can be utilized to tag the overlaid particles, since the IP of the overlay process can have some sizable shift to the IP of the target process. With these information, a multivariate method, BDT here, is implemented to give a likeness of being overlay for each particle. The variables used in BDT are shown in figure 5. The BDT is trained for two categories, neural particles and charged particles. In the former one only Pt and rapidity are used and z_0 is added to

the later one. As stated before, the output of the BDT depicts the likeness of events being beam background overlay, which is shown in figure 6. A relatively large likeness of overlay is required to tag the overlaid particles. This particle based method shows better performance than the jet clustering based method in case of relatively soft jets, such as jets from W^* in the analysis of $H \to WW^*$, as shown in figure 4 (right).

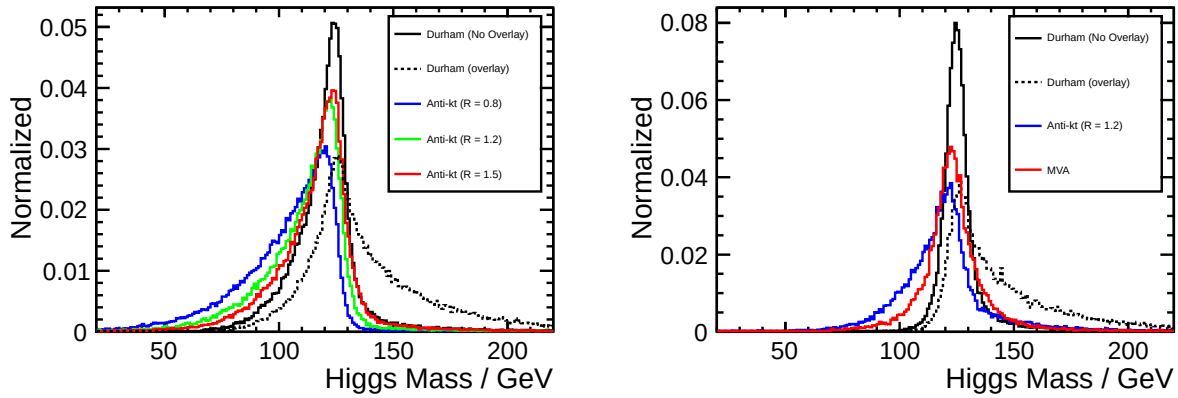

FIG. 4: Comparison of the reconstructed Higgs invariant mass by different options to remove the overlay in case of $H \to b\bar{b}$ (left) and $H \to WW^*$ (right).

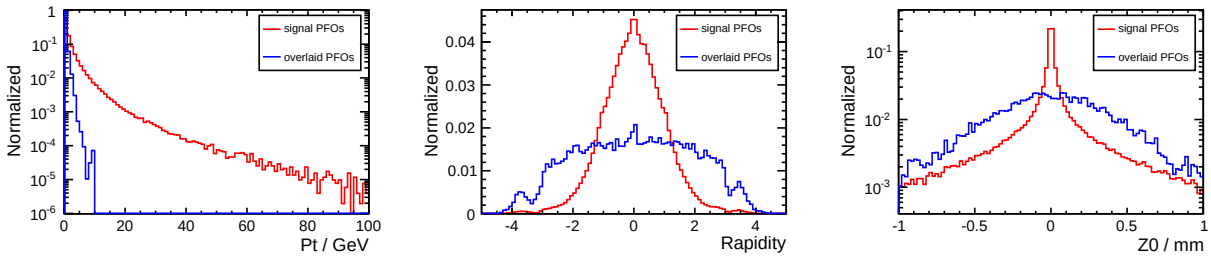

FIG. 5: Distributions of Pt (left), rapidity (middle) and z_0 of IP (right, only for charged) for particles from overlay process or target process.

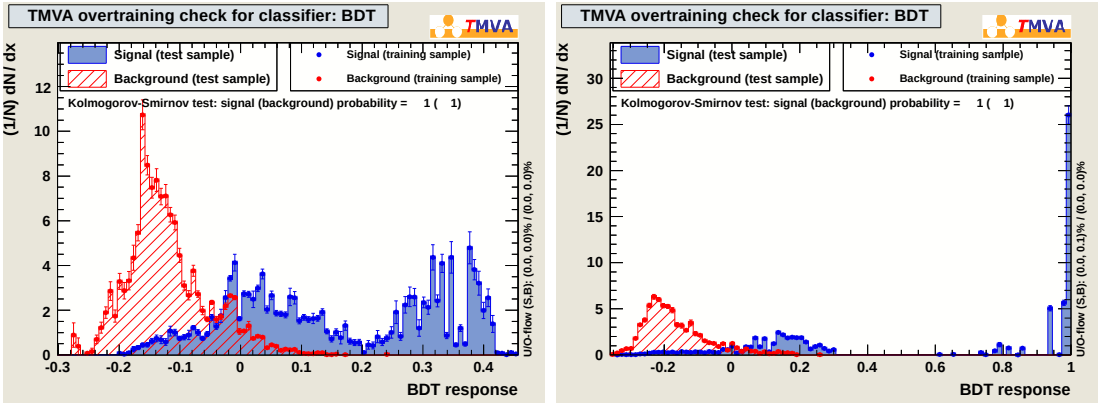
TMVA overtraining check for classifier: BDT
TMVA
Signal (test sample)
Background (test sample)
Signal (training sample)
Background (training sample)
Kolmogorov-Smirnov test: signal (background) probability = 1 (1)
(1/N) dN / dx
U/O-flow (S,B): (0.0, 0.0)% / (0.0, 0.0)%
U/O-flow (S,B): (0.0, 0.1)% / (0.0, 0.0)%
BDT response

FIG. 6: BDT Output for two categories: neutral particles (left) and charged particles (right).

B. Event selection and reduction table

The following steps are carried out orderly in the pre-selection:

- The anti-k_T jet clustering based method is applied to remove the beam induced overlay with R = 1.5, which is implemented by the package FastJetClustering.
- An event is rejected if any isolated charged lepton is found.
- After the overlay removal, the remaining particles are clustered into two jets, each of which is flavor tagged. This step is implemented by the package LCFIPlus.
- Each jet is required to have at least 8 particles.

The following cuts are applied orderly in the final selection:

- Cut1: the visible energy is required to be smaller than 300 GeV but larger than 100 GeV, and the total Pt is required to be larger than 20 GeV.
- Cut2: the charged lepton with largest momentum ($P(Lmax)$) in the remaining particles is required to have relatively larger cone energy (E_{cone}), which is $P(Lmax) < 2E_{cone} + 20$ GeV.
- Cut3: the b-likenesses of the two jets ($Prob(Jet1)$, $Prob(Jet2)$) are required to be large, $Prob(Jet1) + 2Prob(Jet2) > 0.92$.
- Cut4: the missing mass is required to be larger than 172 GeV.
- Cut5: the reconstructed Higgs invariant mass is required to be larger than 100 GeV but smaller than 143 GeV.

The remaining numbers of signal and background events after each cut are shown in the reduction table II. Eventually, assuming an integrated luminosity of 500 fb^{-1} and a beam polarization of $P(e^-, e^+) = (-80\%, +30\%)$, 29199 signal events of which 28598 are from $H \to b\bar{b}$, and 7176 background events dominated by $\nu\bar{\nu}Z$ and ZH are selected. The statistical significance is 150σ and the relative precision of $\sigma_{\nu\bar{\nu}H} \times \mathrm{Br}(H \to b\bar{b})$ at 500 GeV is expected to be 0.667%, which is consistent with what extrapolated from LoI results in DBD of 0.661%.

TABLE II: The reduction table for signal and backgrounds in the analysis of $\nu\bar{\nu}H \to \nu\bar{\nu}b\bar{b}$ at 500 GeV. The cut names are explained in text. $\nu\bar{\nu}H$ has two types, one of signal WW-fusion process, the other from ZH process. The number of signal events after Cut5 in the parenthesis is for $H \to b\bar{b}$.

Process	expected	pre-selection	Cut1	Cut2	Cut3	Cut4	Cut5
$\nu\bar{\nu}H$(fusion)	7.47×10^4	59698	54529	54048	35598	34278	299199 (28598)
$\nu\bar{\nu}H(ZH)$	1.02×10^4	7839	7301	7224	4863	1951	1512
4f_sznu_sl	2.79×10^5	234259	203489	202977	44943	39125	3957
4f_sw_sl	2.43×10^6	228436	135164	121791	1495	911	132
4f_zz_sl	1.83×10^5	102172	60684	59865	13036	5736	461
4f_ww_sl	2.78×10^6	653997	287428	250944	3851	1145	176
4f_sze_sl	9.41×10^5	65011	1311	1259	91.1	40.7	5.51
6f_yyveev	6.05×10^3	931	306	104	96.6	87.4	20.4
6f_yyvelv	2.37×10^4	5450	2425	1116	997	907	237
6f_yyvllv	2.36×10^4	8009	4272	2813	2556	2383	674
BG	6.68×10^6	1.31×10^6	702379	648094	71929	52285	7176
significance	16.6	35.0	43.3	44.6	106	114	150

V. ANALYSIS OF $\sigma_{\nu\bar{\nu}H} \times \mathrm{Br}(H \to WW^*)$ @ 500 GEV

Depending on the decay mode of each W, two analyses are carried focusing on full hadronic and semi-leptonic decays of WW^*.

A. $WW^* \to$ 4-jets

In this mode, the final state consists of two missing neutrinos and four jets none of which is a b-jet. In the pre-selection, it is essential to reconstruct the four jets and to pair them according to one on-shell W and one off-shell W^*. Then the Higgs mass can be fully reconstructed. The main background processes considered here are similar to those in the $H \to b\bar{b}$ analysis, dominated by $\nu\bar{\nu}Z$, $e\nu W$ and W^+W^-.

The following steps are carried out orderly in the pre-selection:

- The particles based method is applied to remove the beam background overlay, which is implemented according to the method in IV-A.
- An event is rejected if any isolated charged lepton is found.
- After the overlay removal, remaining particles are clustered into four jets, each of which is flavor tagged. This step is implemented by the package LCFIPlus.
- Due to the jets originating from off-shell W^*, the number of particles in each jet, which are ordered by the energy from largest to smallest, is required to be no smaller than 7, 6, 5, 4, and in total the number of particles need be no smaller than 40.

The following cuts are applied orderly in the final selection:

- Cut1: the Y values obtained from jet clustering should match the features of four jet events in order to suppress backgrounds with fewer partons such as $\nu\bar{\nu}Z \to \nu\bar{\nu}qq$, $e\nu W \to e\nu qq$, or $W^+W^- \to \nu\bar{\nu}qq$. Nevertheless, one should keep in mind that no perfect jet clustering algorithm here can reject all the two partons events. The Y values are required to satisfy $Y_{4\to3} > 0.0026$ and $Y_{3\to2} > 0.0076$.
- Cut2: the visible energy is required to be smaller than 230 GeV, total Pt is required to be larger than 20 GeV and the missing mass is required to be larger than 200 GeV, which significantly suppresses the contribution from ZH.
- Cut3: the charged lepton with largest momentum ($P(Lmax)$) in the remaining particles is required to have relatively larger cone energy (E_{cone}), which is $P(Lmax) < 2E_{cone} + 9$ GeV.
- Cut4: to suppress events with b-jets, such as $H \to b\bar{b}$, $t\bar{t}$, etc., the b-likenesses of the four jets (sorted from largest to smallest $btag1$, $btag2$, $btag3$, $btag4$) are required to satisfy $btag1 + 2btag2 < 0.7$ and $btag3 + 2btag4 < 0.14$.
- Cut5: the reconstructed on-shell W mass is required to be larger than 54 GeV but smaller than 94 GeV, the off-shell W^* mass is required to be smaller than 64 GeV but larger than 11 GeV.
- Cut6: the reconstructed Higgs invariant mass is required to be larger than 114 GeV but smaller than 142 GeV.

The reconstructed Higgs invariant mass after the first five cuts is depicted in figure 7. The remaining numbers of signal and background events after each cut are listed in the reduction table III. Eventually, by assuming an integrated luminosity of 500 fb^{-1} and a beam polarization of $P(e^-, e^+) = (-80\%, +30\%)$, 4945 signal events of which 3136 are from $H \to WW^*$ and 3055 background events dominated by $\nu\bar{\nu}Z$, $e\nu W$ and W^+W^- are selected. The statistical significance is 35σ and the relative precision of $\sigma_{\nu\bar{\nu}H} \times \mathrm{Br}(H \to WW^*)$ is expected to be 2.8%.

B. $WW^* \to l\nu +$ 2-jets

In this mode, the final state consists of three missing neutrinos, one isolated charged lepton and two jets. In the pre-selection, it is essential to find the isolated charged lepton and to reconstruct the two jets. One W can be fully reconstructed from the two jets. However the other W cannot be fully reconstructed from the isolated charged lepton and one missing neutrino due to the other two missing neutrinos originating from WW-fusion. Hence, the Higgs mass cannot be fully reconstructed either. The main background processes considered here are similar to those in the $WW^* \to$ 4-jets analysis, dominated by $W^+W^- \to l\nu qq$.

The following steps are carried out orderly in the pre-selection:

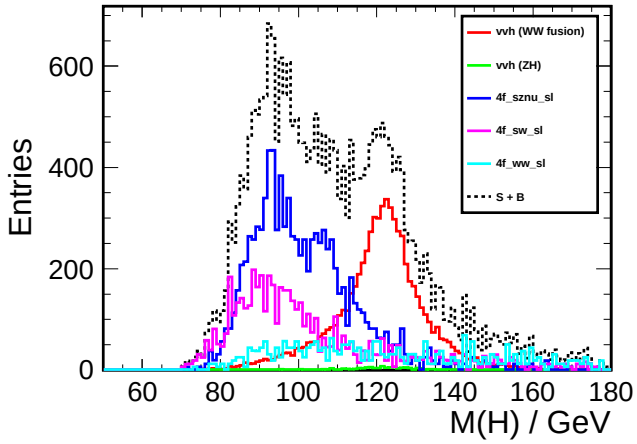

FIG. 7: Distribution of the reconstructed Higgs invariant mass using the fully hadronic mode of $H \to WW^*$.

TABLE III: The reduction table for the signal and backgrounds in the analysis of $\nu\bar{\nu}H \to \nu\bar{\nu}WW^* \to \nu\bar{\nu} + 4$-jets at 500 GeV. The cut names are explained in text. $\nu\bar{\nu}H$ has two types, one of signal WW-fusion process, the other from ZH process. The number of signal events after Cut6 in the parenthesis is for $H \to WW^*$.

Process	expected	pre-selection	Cut1	Cut2	Cut3	Cut4	Cut5	Cut6
$\nu\bar{\nu}H$(fusion)	7.47×10^4	42373	14461	11684	11315	7415	6746	4970(3136)
$\nu\bar{\nu}H(ZH)$	1.02×10^4	5497	911	240	232	144	120	86.8
4f_sznu_sl	2.79×10^5	140092	23016	18123	17841	14157	9675	1308
4f_sw_sl	2.43×10^6	220670	40715	11746	11383	11013	5317	778
4f_zz_sl	1.83×10^5	57640	7041	722	690	546	342	65.1
4f_ww_sl	2.78×10^6	416386	46390	4816	4149	3934	2965	806
4f_sze_sl	9.41×10^5	45911	19160	38.4	38.4	32.1	8.56	0
6f_yyveev	6.05×10^3	52.5	35.7	9.24	0.02	0	0	0
6f_yyvelv	2.37×10^4	703	498	102	45.6	9.51	5.78	3.88
6f_yyvllv	2.36×10^4	2025	1420	358	252	30.4	26.6	7.60
BG	6.68×10^6	8.89×10^5	139185	36156	34632	29866	18462	3055
significance	3.0	6.8	13.4	19.4	19.5	21.0	24.6	35.0

- Select events with one isolated electron or muon from all particles, otherwise the event is rejected.
- The particles based method is applied to remove the beam background overlay, which is implemented according to the method used in IV-A.
- The remaining particles are clustered into two jets, each of which is flavor tagged. This step is implemented by the package LCFIPlus.
- To suppress events in which the reconstructed jets are actually τ-jets, each jet is required to have at least two charged particles with relatively high Pt (> 500 MeV).

The following strategies are used in the final selection:

- depending on the type of the selected isolated charged lepton, all events are separated into two categories, electron-type or muon-type. This is due to background contamination and hence the cut optimization is very different for these two categories.
- large missing energy and large missing Pt are required to suppress the fully hadronic backgrounds.
- the b-likenesses of the two jets are required to be small to suppress backgrounds with b-jets.
- to suppress the dominant background $W^+W^- \to l\nu qq$, the angle between reconstructed W from two jets and isolated charged lepton is required to be relatively small.

- in case of the electron-type category, the polar angle of the electron is required to be not close to beam direction to suppress the eeZ and $e\nu W$ backgrounds; the angle between electron and each of the two jets is required to be relatively large since the selected electron can be a mis-identified electron from the jets.
- the partially reconstructed Higgs invariant mass ($m(lqq)$) is still useful to further suppress the backgrounds.

The fully reconstructed W mass from the two jets, as well as the partially reconstructed Higgs mass from the lepton and two jets are shown in figure 8. The remaining numbers of signal and background events after all cuts are shown in the reduction table IV for both categories. Eventually, by assuming an integrated luminosity of 500 fb^{-1} and a beam polarization of $P(e^-, e^+) = (-80\%, +30\%)$, the statistical significance for the muon-type category is 17.4σ and 14.7σ for the electron-type. The combined result is 22.8σ. The relative precision of $\sigma_{\nu\bar{\nu}H} \times \mathrm{Br}(H \to WW^*)$ is expected to be 4.4% using the semi-leptonic decay mode of WW^*.

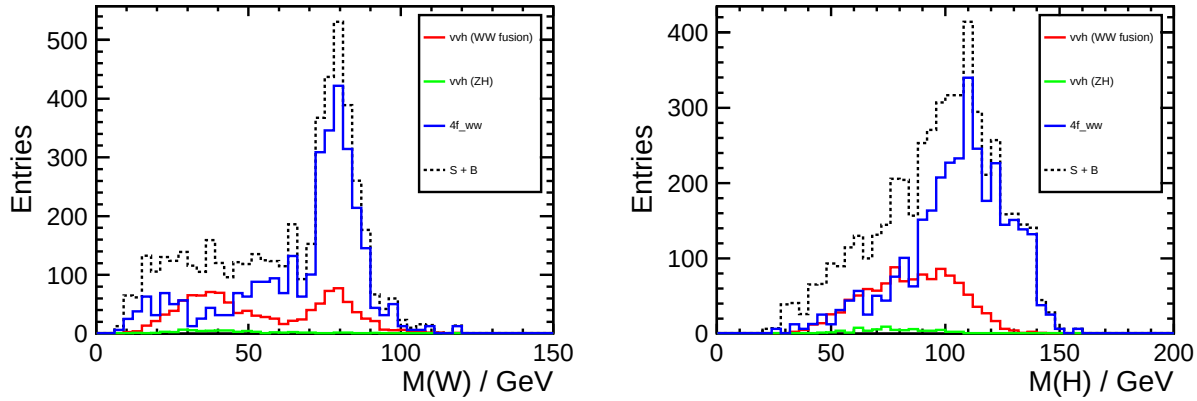

FIG. 8: Distribution of fully reconstructed W mass (left) and partially reconstructed Higgs mass (right) using the semi-leptonic mode $H \to WW^*$.

TABLE IV: The remaining numbers of signal and background events for the two categories in the analysis of $\nu\bar{\nu}H \to \nu\bar{\nu}WW^* \to \nu\bar{\nu} + l\nu + 2$-jets at 500 GeV. The number of signal events in the parenthesis is for $H \to WW^*$.

category	signal	background	significance
muon-type	1002 (982)	2187	17.4σ
electron-type	879 (858)	2528	14.7σ

C. Combined of $H \to WW^*$ with full hadronic and semi-leptonic modes

By combining the two decay modes of WW^*, the relative precision of $\sigma_{\nu\bar{\nu}H} \times \mathrm{Br}(H \to WW^*)$ at 500 GeV is expected to be 2.4%, assuming an integrated luminosity of 500 fb^{-1} and a beam polarization of $P(e^-, e^+) = (-80\%, +30\%)$.

VI. SUMMARY

The relative precision of $\sigma_{\nu\bar{\nu}H} \times \mathrm{Br}(H \to b\bar{b})$ at 250 GeV is expected to be 10.5% with 250 fb^{-1} data, and at 500 GeV is expected to be 0.667% with 500 fb^{-1} data, assuming beam polarisations $P(e^-, e^+) = (-80\%, +30\%)$ at both energies. The Higgs total width is expected to be measured with precision of 13% at 250 GeV according to Option B, and 5.4% at 500 GeV according to Option A. By adding $H \to ZZ^*$ and other decay modes [22], the expected precision of Higgs total width at 250 GeV only is 11%, and by combining 250 GeV and 500 GeV data is 5.0%. HWW coupling can be determined to a precision of 4.8% at 250 GeV and 1.2% at 500 GeV with the baseline luminosities of ILC. The results are summarized in Table V, where the expectations with luminosity upgrade scenarios [23] of ILC are also shown. The capability of sub-percent level measurement of HWW coupling will be crucial to hint at next energy scale of new physics beyond SM.

$\Delta g/g$	Baseline		LumiUP	
	250 GeV	+ 500 GeV	250 GeV	+ 500 GeV
g_{HWW}	4.8%	1.2%	2.3%	0.58%
Γ_H	11%	5%	5.4%	2.5%

TABLE V: Expected precisions of total Higgs width and HWW coupling for both baseline and luminosity upgrade (LumiUP) scenarios of ILC, at 250 GeV and 500 GeV, where the data at earlier stage is combined to later stage.

Acknowledgments

We would like to thanks all the members of the ILC physics subgroup and ILD optimization group for useful discussions, particularly to the software group T. Barklow, M. Berggren, A. Miyamoto and F. Gaede for preparing all the samples. This work is supported in part by the Creative Scientic Research Grant No. 18GS0202 of the Japan Society for Promotions of Science (JSPS), the JSPS Grant-in-Aid for Science Research No. 22244031, and the JSPS Specially Promoted Research No. 23000002.

[1] Bogdan A. Dobrescu and Joseph D. Lykken. Coupling spans of the Higgs-like boson. *JHEP*, 1302:073, 2013, 1210.3342.
[2] Vernon Barger, Muneyuki Ishida, and Wai-Yee Keung. Total Width of 125 GeV Higgs Boson. *Phys.Rev.Lett.*, 108:261801, 2012, 1203.3456.
[3] Fabrizio Caola and Kirill Melnikov. Constraining the Higgs boson width with ZZ production at the LHC. 2013, 1307.4935.
[4] Howard Baer, Tim Barklow, Keisuke Fujii, Yuanning Gao, Andre Hoang, et al. The International Linear Collider Technical Design Report - Volume 2: Physics. 2013, 1306.6352.
[5] A. Djouadi, J. Kalinowski, and M. Spira. HDECAY: A Program for Higgs boson decays in the standard model and its supersymmetric extension. *Comput.Phys.Commun.*, 108:56–74, 1998, hep-ph/9704448.
[6] A. Djouadi. Higgs particles at future hadron and electron - positron colliders. *Int.J.Mod.Phys.*, A10:1–64, 1995, hep-ph/9406430.
[7] Wai-Yee Keung and William J. Marciano. HIGGS SCALAR DECAYS: H to W+- X. *Phys.Rev.*, D30:248, 1984.
[8] H. Li et al. HZ Recoil Mass and Cross Section Analysis in ILD. 2012, 1202.1439.
[9] Hiroaki Ono and Akiya Miyamoto. A study of measurement precision of the Higgs boson branching ratios at the International Linear Collider. *Eur.Phys.J.*, C73:2343, 2013, 1207.0300.
[10] Hiroaki Ono. Higgs branching fractions study in ILC. 2012. Presentation at KILC12 Workshop.
[11] J.F. Gunion, H.E. Haber, and J. Wudka. Sum rules for Higgs bosons. *Phys.Rev.*, D43:904–912, 1991.
[12] Koji Tsumura. What if the Higgs coupling deviates from the SM one. 2013. Presentation at LCWS13.
[13] T. Behnke, J. E. Brau, P. N. Burrows, J. Fuster, M. Peskin, M. Stanitzki, Y. Sugimoto, S. Yamada, and H. Yamamoto. The International Linear Collider Technical Design Report - Volume 4: Detectors. *ArXiv e-prints*, June 2013, 1306.6329.
[14] Toshinori Abe et al. The International Large Detector: Letter of Intent. 2010, 1006.3396.
[15] Wolfgang Kilian, Thorsten Ohl, and Jurgen Reuter. WHIZARD: Simulating Multi-Particle Processes at LHC and ILC. *Eur.Phys.J.*, C71:1742, 2011, 0708.4233.
[16] P. Mora de Freitas and H. Videau. Detector simulation with MOKKA / GEANT4: Present and future. Prepared for International Workshop on Linear Colliders (LCWS 2002), Jeju Island, Korea, 26-30 Aug 2002.
[17] F. Gaede. Marlin and LCCD: Software tools for the ILC. *Nucl. Instrum. Meth.*, A559:177–180, 2006.
[18] M.A. Thomson. Particle Flow Calorimetry and the PandoraPFA Algorithm. *Nucl.Instrum.Meth.*, A611:25–40, 2009, 0907.3577.
[19] Taikan Suehara, Tomohiko Tanabe, and Satoru Yamashita. Improved jet clustering algorithm with vertex information for multi-bottom final states. 2011, 1110.5785.
[20] : David Bailey et al. The LCFIVertex package: vertexing, flavour tagging and vertex charge reconstruction with an ILC vertex detector. *Nucl. Instrum. Meth.*, A610:573–589, 2009, 0908.3019.
[21] Pisin Chen, Timothy L. Barklow, and Michael E. Peskin. Hadron production in gamma gamma collisions as a background for e+ e- linear colliders. *Phys.Rev.*, D49:3209–3227, 1994, hep-ph/9305247.
[22] Junping Tian and Keisuke Fujii. Summary of Higgs coupling measurements with staged running of ILC at 250 GeV, 500 GeV and 1 TeV. 2013. LC-REP-2013-021.
[23] D.M. Asner, T. Barklow, C. Calancha, K. Fujii, N. Graf, et al. ILC Higgs White Paper. 2013, 1310.0763.